

Synthesis and investigation of a tris-cyclometalated iridium complex bearing a single quarternary ammonium group

Sureemas Meksawangwong^a, Bhavini Gohil^b, Wikorn Punyain^a, Robert Pal^b Filip Kielar^{*a}

- a) Department of Chemistry and Center of Excellence in Biomaterials, Faculty of Science, Naresuan University, Phitsanulok 65000, Thailand
- b) Department of Chemistry, Durham University, South Road, Durham, DH1 3LE, UK

Abstract

A novel tris-cyclometalated iridium complex (**1**) containing a single quarternary ammonium moiety has been synthesized, characterized, and investigated as a potential cellular imaging probe. The complex is the next generation of the aminoalkyl iridium complexes recently published by our group. The complex possesses outstanding photophysical properties. The complex is stable in solution in dark but exhibits rapid photocatalyzed transformations. Investigations of this behavior have shown that these transformations involve the formation of an electrophilic species, which can be captured by a suitable nucleophile, leading to the formation of new product. The complex has also been investigated as a potential cellular stain. It is less cytotoxic than its aminoalkyl predecessor and shows lysosomal localization as its precursor.

Keywords

Iridium; Cellular Imaging; Photochemistry

Corresponding Author:
Filip Kielar
Department of Chemistry
Naresuan University
Phitsanulok
65000
Thailand
filipkielar@nu.ac.th

Introduction

Cyclometalated photoactive iridium complexes have received significant amount of attention recently, due to their interesting and biologically favoured photophysical properties.[1, 2] They have found uses in applications ranging from cellular imaging to organic light emitting devices, and photoredox catalysts.[1, 3-6] The remarkable photophysical properties of these compounds are mainly the result of the very large ligand-field splitting energy and very high spin-orbit coupling constant.[2, 7-9] The first of these, derives from the combination of the strong σ -donating character of the cyclometalating ligands, the high charge of the Ir^{3+} ion, and overall size of the 5d orbitals.[2] It ensures that pure d-d transitions are unfavorable and electronic states containing ligand character are thus involved in the photochemistry of these compounds.[2, 9] Ultimately this results in rich photochemical properties dominated by charge transfer transitions such as metal-to-ligand charge-transfer (MLCT) or ligand-to-ligand charge-transfer (LLCT).[7, 10] The high spin-orbit coupling constant in turn ensures efficient involvement of triplet excited states as it relaxes the forbidden nature of singlet-to-triplet transitions. Thus, for example, the photoluminescence lifetimes of cyclometalated iridium complexes commonly reach values in the microsecond regime, which is significantly higher than for organic fluorophores, but shorter than observed for phosphorescence from organic structures.[7] Finally, the fact that the HOMO and LUMO orbitals of cyclometalated iridium complexes are usually located on different parts of the molecule enables fairly facile tuning of emission colors as the energies of the orbitals can be altered by structural modification in a relatively independent fashion.[11, 12]

In terms of cellular imaging, the beneficial features of cyclometalated iridium complexes include the above mentioned relatively long luminescence lifetimes, large Stokes' shifts, and the possibility for the emission properties to be modulated by various stimuli.[13] The first two of these enable improved separation of the signal arising from the iridium complex being used as a probe from unwanted background bioautofluorescence.[9, 14, 15] Whilst modulation of the emission allows to create responsive probes that are currently in high demand.[16, 17]

The most common structural type of cyclometalated iridium complexes utilized in cellular imaging are bis-cyclometalated iridium complexes, which contain two cyclometalating C^N (e.g. 2-phenylpyridine, ppy) ligands and one diimine N^N ligand (e.g. 2,2'-bipyridine, bpy).[9] These complexes possess positive charge, which likely aids their cellular uptake. A second common structural type are tris-cyclometalated iridium complexes possessing three cyclometalating C^N ligands, which are charge neutral. These complexes have seen significantly less utilization in cellular imaging than the bis-cyclometalated ones.[9, 18, 19]

Our group has recently published a report on two simple derivatives of the prototypical tris-cyclometalated iridium complex *fac*-[Ir(ppy)₃] which contained simple aminoalkyl substituents on one of the ppy ligands.[20] These complexes have been demonstrated to possess photochemical properties similar to that of their parent structure and have been shown to label live cells. Their ability to stain live cells was in part ascribed to the fact that the amino group will be protonated in biological media thus giving them a positive charge aiding their uptake. We have, therefore, envisaged that transforming such aminoalkyl complexes into their respective quaternary ammonium salts should result in

structures that would also be taken up by cells and could be used as cellular probes. Herein, we describe the synthesis, photochemical investigation, and cellular imaging experiments with one such derivative.

Experimental

General comments

Unless otherwise stated, all commercial reagents were used as received. Silver trifluoromethanesulfonate, N-tetrabutylammonium hexafluorophosphate, and sodium borohydride were purchased from Sigma Aldrich. Sodium cyanoborohydride, 2-phenylpyridine (ppy), 2-ethoxyethanol, and silicagel were purchased from Merck. Butylamine, methyl iodide, and iridium(III)chloride trihydrate were purchased from Fisher. Dichloromethane, methanol, and triethyl amine were purchased from Carlo Erba. Sodium bicarbonate, anhydrous sodium sulphate, and trisodium phosphate were purchased from Univar. Acetonitrile and dimethyl sulfoxide were purchased from RCI. The precursor complex [Ir(ppy)₂(ppy-Me-NC₄)] was synthesized as previously reported.[20] ¹H and ¹³C NMR spectra were recorded on a Bruker Avance 400 MHz instrument operating at 400 MHz and 100 MHz for proton and carbon, respectively. Mass spectra were recorded with an Agilent technologies UHD Accurate-Mass Q-TOF LC-MS instrument model 6540. UV-Visible spectra were recorded using Analytik Jena 210plus diode array spectrophotometer. Steady state emission spectra were recorded using Fluoromax-4 spectrofluorometer from Yvon Horiba. Phosphorescence lifetime measurements were performed on the DeltaFlex™ instrument equipped with a UV LED ($\lambda_{ex} = 372$ nm). Cell viability was determined using the Chemometec NucleoCounter3000 cell analyzer.

Synthesis of iridium complex **1**

[Ir(ppy)₂(ppy-Me-NC₄)] (300 mg, 0.79 mmol), methyl iodide (0.15 mL, 2.38 mmol), and potassium carbonate (109 mg, 0.79 mmol) were suspended in acetonitrile 20 mL. The reaction mixture was heated to reflux for 24 h. The reaction mixture was allowed to cool down and the solvent was removed under reduced pressure. The residue was recrystallized using dichloromethane and hexane to yield the product as a yellow solid; 248 mg (0.32 mmol, 80%). ¹H NMR (400 MHz, DMSO-*d*₆, δ) 0.86 (t, *J* = 7.6 Hz, 3H), 1.17 (m, 2H), 1.53 (m, 2H), 2.81(s, 3H), 2.82 (s, 3H), 3.03 (m, 2H), 4.16 (m, 2H), 6.55 (d, *J* = 7.6 Hz, 1H), 6.62-6.73 (m, 4H), 6.82 (m, 2H), 6.97 (d, *J* = 8.0 Hz, 1H), 7.20 (m, 2H), 7.21 (m, 1H), 7.49 (m, 2H), 7.55 (d, *J* = 4.8 Hz, 1H), 7.75-7.88 (m, 5H), 7.90 (d, *J* = 8.0 Hz, 1H), 8.14 (d, *J* = 8.8 Hz, 2H), 8.24 (d, *J* = 8.4 Hz, 1H). ¹³C NMR (100 MHz, DMSO-*d*₆, δ) 13.5, 19.3, 23.6, 49.4, 62.0, 67.3, 119.1, 119.9, 123.0, 123.8, 124.3, 127.9, 129.2, 136.0, 137.1, 140.1, 143.7, 143.9 146.2, 146.9, 147.2, 159.8, 160.0, 161.4, 164.5, 165.4. HRMS (ES⁺) calcd. for C₄₀H₄₀IrN₄ (769.2877); found (769.2896).

Photochemical measurements

Unless otherwise stated, stock solutions of iridium complexes (0.5 mM) were prepared in DMSO. They were then diluted to their desired concentration (typically 10 μ M) with the appropriate solvent. The measurements were performed in quartz cuvettes of 1 cm path length. Degassing of the samples for lifetime measurements have been achieved by

bubbling nitrogen gas through them for 10 minutes in order to eliminate the presence of oxygen.

Luminescence quantum yields were determined using *fac*-[Ir(ppy)₃] in degassed dichloromethane solution as the standard, for which $\Phi_{\text{lum}} = 0.40$. The solutions for this measurement were degassed by four cycles of freeze-pump-thaw.

Luminescence lifetimes of the complexes were measured by time-correlated-single-photon-counting (TCSPC) using a laser diode (372 nm) as the excitation source. The estimated error in the lifetimes is 10%.

DFT Calculations

Calculations were carried out with the Gaussian09 software package at the DFT level, using the hybrid functional B3LYP and the double-zeta basis set LANL2DZ.[21] The calculations were carried out for a vacuum environment as well dichloromethane ($\epsilon = 8.93$) using the polarizable continuum model. The molecular orbitals were visualized using the Gabeit program package.[22]

Photoreaction A (Phototransformation in pure solvents)

Solution of complex **1** (10 mg, 0.011 mmol) in a suitable solvent (5 mL) was placed in a scintillation vial and left at ambient conditions in the laboratory or illuminated by a household LED lamp for the specified amount of time. The reaction mixture was analyzed by mass spectrometry. Control reactions were carried out by placing the solutions in a cupboard to avoid exposure to light.

Photoreaction B (Phototransformation in the presence of added nucleophiles)

Solution of complex **1** (10 mg, 0.011 mmol) and a nucleophile of choice (0.055 mmol) in dichloromethane (5 mL) were placed in a scintillation vial and illuminated by a household LED lamp for the specified amount of time. The reaction mixture was analyzed by mass spectrometry.

Cell Culture

A detailed investigation of the cellular behaviour of each complex was conducted using mouse skin fibroblasts (NIH-3T3) and human prostate adenocarcinoma (PC3) cell lines using fluorescence and laser scanning confocal microscopy. Cells were maintained in exponential growth as monolayers in F-12/DMEM (Dulbecco's Modified Eagle Medium) 1:1 that was supplemented with 10% foetal bovine serum (FBS). Cells were grown in 75 cm² plastic culture flasks, with no prior surface treatment. Cultures were incubated at 37 °C, 20% average humidity and 5% (v/v) CO₂. Cells were harvested by treatment with 0.25% (v/v) trypsin solution for 5 min at 37 °C. Cell suspensions were pelleted by centrifugation at 1000 rpm for 3 min and were re-suspended by repeated aspiration with a sterile plastic pipette. Microscopy Cells were seeded in 12-well plates on 13mm 0.170mm thick standard glass coverslips or un-treated iBibi 100 uL live cell channels and allowed to grow to 40% – 60% confluence, at 37 °C in 5% CO₂. At this stage, the medium was replaced and cells were treated with complexes and co-stains as appropriate. For imaging DMEM media (10% FBS) lacking phenol red (live cell media) was used from this point onwards. Following incubation, the cover-slips were washed with live cell media,

mounted on slides and the edges sealed with colourless, quick-dry nail varnish to prevent drying out of the sample.

Cell toxicity measurements were run using a ChemoMetec A/S NucleoCounter3000-Flexicyte instrument with Via1-cassette cell viability cartridge (using the cell stain Acridine Orange for cell detection, and the nucleic acid stain DAPI for detecting non-viable cells). The experiments were done in triplicate. In cellular uptake studies Cells were seeded in 6-well plates and allowed to grow to 80% – 100% confluence, at 37 °C in 5% CO₂. At this stage, the medium was replaced with media containing targeted complexes as detailed above and total cellular Iridium was determined using ICP-MS, inductively coupled plasma mass spectrometry by Dr. C. Ottley in the Department of Earth Sciences at Durham University.

Steady state fluorescence and multiphoton microscopy

Steady state fluorescence images were recorded using a PhMoNa[23] enhanced Leica SP5 II LSCM confocal microscope equipped with a HCX PL APO 63x/1.40 NA LambdaBlue Oil immersion objective. Data were collected using 2.5x digital magnification at 400 Hz/line scan speed (4 line average, bidirectional scanning) at 355 nm (3rd harmonic NdYAG laser) with 3 mW laser power (80 nJ/voxel). In order to achieve excitation with maximal probe emission, the microscope was equipped with a triple channel imaging detector, comprising a conventional PMT systems and two HyD hybrid avalanche photodiode detector. The latter part of the detection system, when operated in the BrightRed mode, is capable of improving imaging sensitivity by 25%, reducing signal to noise by a factor of 5. Frame size was determined at 2048 x 2048 pixel, with 0.6 airy disc unit determining the applied pinhole diameter rendering on voxel to be corresponding to 24.02 x 24.02 nm (frame size 49.16 x 49.16 µm) with a section thickness of 380 nm. A HeNe or Ar ion laser was used when commercially available organelle-specific stains (e.g. MitoTrackerRed™) were used to corroborate cellular compartmentalization. Spectral imaging on this Leica system is possible with the $xy\lambda$ -scan function, using the smallest allowed spectral band-pass (5nm) and step-size (3nm) settings. However, much improved spectral imaging in cells was achieved using a custom built microscope (modified Zeiss Axiovert 200M), using a Zeiss APOCHROMAT 63x/1.40 NA objective combined with a low voltage (5 V) 365 nm pulsed UV LED focused, collimated excitation source (1.2W). For rapid spectral acquisition the microscope was equipped at the X1 port with a Peltier cooled 2D-CCD detector (Ocean Optics, MayaPro) used in an inverse 100 Hz time gated sequence. The spectrum was recorded from 400-800 nm with a resolution of 0.24 nm and the final spectrum was acquired using an averaged 10,000 scan duty cycle. Probe lifetimes were measured on the same microscope platform using a novel cooled PMT detector (Hamamatsu H7155) interchangeable on the X1 port, with the application of pre-selected interference filters matched to as selected in live cell LSCM experiments. Both the control and detection algorithm were written in LabView2013, where probe lifetime was determined by using a single exponential fitting algorithm to the monitored signal intensity decay.

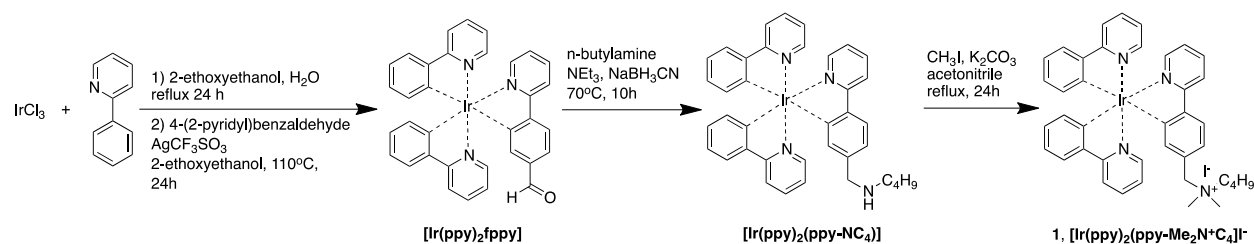
Multiphoton microscopy has been conducted on three instruments at two locations. At Durham (Department of Biosciences) a Nikon E600 upright microscope equipped with a BioRad MicroRadiance 2000 Multiphoton head coupled to a Spectra-Physics MaiTai tunable (710-980 nm, 80 mW @ 720 nm, 80 MHz, 100 fs) multiphoton laser using a x60

1.4NA water immersion IR objective (operating at 166 lines/s scan speed and 512 × 512 pixel FOV) has been used.

The threshold algorithm to control brightness automated by the BioRad MicroM is calculated by the image specific signal-to-noise ratio or it is accessible post image-processing *via* imageJ 1.49h.

Results and discussion

Synthesis



Scheme 1. Synthesis of complex **1**

Complex **1** ($\text{fac-}[\text{Ir}_2(\text{ppy})_2(\text{ppy-Me}_2\text{N}^+\text{C}_4)]\text{I}$) was prepared in four steps as shown in **Scheme 1**. The first three steps were adopted from the literature and involve the synthesis of the chloride bridged dimer using the Nonoyama reaction, conversion of this dimer into $\text{fac-}[\text{Ir}(\text{ppy})_2\text{fppy}]$ using 4-(2-pyridyl)benzaldehyde, and the reductive amination of the formyl group to yield $\text{fac-}[\text{Ir}(\text{ppy})_2(\text{ppy-NC}_4)]$. [20, 24, 25] Complex **1** was then made in the final step by quaternization of the secondary amino group using methyl iodide as the alkylating agent. Attempts to purify complex **1** using column chromatography were not successful and the purification had to be performed using recrystallization. The inability to perform the purification of complex **1** using column chromatography alerted us to the possibility of its instability. This suspicion was later confirmed when a sample for NMR analysis has been left on the bench for 48 h in d_6 -DMSO where the subsequent $^1\text{H-NMR}$ indicated the formation of the precursor complex $\text{fac-}[\text{Ir}(\text{ppy})_2\text{fppy}]$. It was later established, as will be discussed below, that this transformation was induced by light and therefore solutions for spectroscopic and imaging work were freshly prepared and kept in dark at all times.

Photophysical properties

Absorption and emission spectra of complex **1** were measured in dichloromethane and are shown in **Figure 1**. The UV-Vis absorption spectrum is typical for cyclometalated iridium complexes. There are three main features in this spectrum. The first is a peak with a maximum at 286 nm, which can be attributed to ligand centered π - π^* transitions. The second feature is a peak with maximum at 365 nm, which can be attributed to spin-allowed metal to ligand charge transfer ($^1\text{MLCT}$) transitions. The final feature is a tail extending beyond 500 nm corresponding to forbidden metal to ligand charge transfer ($^3\text{MLCT}$) transitions. The emission spectrum of complex **1** in dichloromethane, recorded after excitation at 390 nm, is also similar to analogous triscyclometalated iridium complexes showing a maximum at 515 nm (**Figure 1**). These spectral properties are

analogous to both the parent compound *fac*-[Ir(ppy)₃] as well as the precursor complex *fac*-[Ir(ppy)₂(ppy-NC₄)] previously reported by our group.

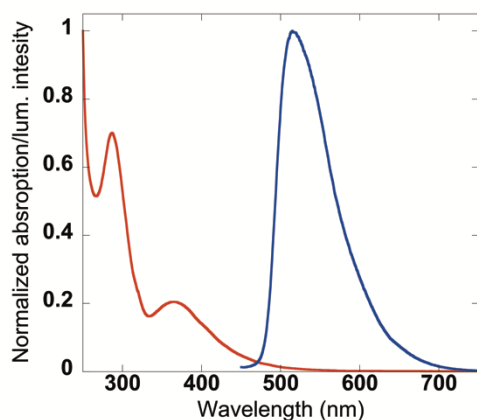


Figure 1. Normalized absorption (red) and emission spectra of complex **1** (10 μ M) recorded in dichloromethane ($\lambda_{\text{ex}} = 390$ nm)

The emission spectrum of complex **1** in aqueous solution is also similar to that observed for the precursor complex with features observed at 527 and 588 nm (**Figure 2**). Emission spectrum for complex **1** was also collected at 77 K and can be seen in **SI Figure 4**.

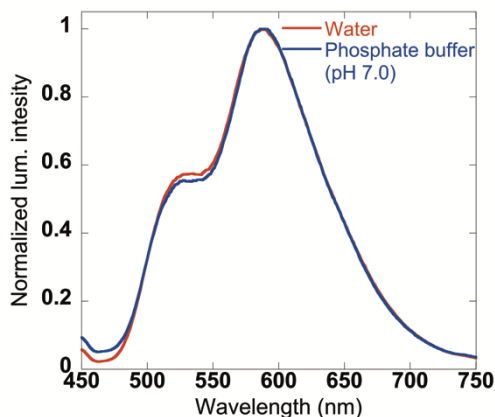


Figure 2. Normalized emission spectra of complex **1** in water (red) and pH 7.0 phosphate buffer (blue) ($\lambda_{\text{ex}} = 390$ nm)

Further characterization of the photophysical properties of complex **1** was performed using time resolved measurements. These measurements were first carried out in organic solvents (dichloromethane and tetrahydrofuran) where the emission intensity decays were monoexponential. These measurements have revealed that in aerated dichloromethane and tetrahydrofuran the lifetimes are 63 (\pm 6.3) and 35 (\pm 3.5) ns, respectively. These values are comparable to those observed for the precursor amine

complex. On the other hand, the lifetime values of 739 (\pm 74) ns and 1.03 (\pm 0.10) μ s in degassed dichloromethane and tetrahydrofuran, respectively, are significantly shorter than those observed for the precursor complex.[20] In addition, the photoluminescence quantum yield for complex **1** is only 9%, which is significantly less than observed for either *fac*-[Ir(ppy)₃] or the precursor complex *fac*-[Ir(ppy)₂(ppy-NC₄)]. This, together with the shorter lifetimes indicates additional non-radiative decay pathways for the excited state of complex **1**. Multi exponential decays were observed in aqueous solutions with the longest lifetime being on the order of 300 ns, which is comparable with the precursor complex. The photophysical properties of complex **1** are summarized in **Table 1**

Table 1. Photophysical properties of complex **1**

	1
Absorption (λ_{\max}/nm) ^a	286, 365
Emission (λ_{\max}/nm) ^a	515
Quantum Yield (Φ_{lum}) ^a	0.09
Emission 77K (λ_{\max}/nm) ^b	513, 549, 590, 649
Lifetime (ns) ^a	739
Lifetime (ns) ^c	1030

a) dichloromethane, b) dimethylsulfoxide, c) tetrahydrofuran

The precursor amine complex exhibited a ratiometric response to pH. This was explained by the effect of protonation/deprotonation of the amino group on the propensity of the complex to aggregate. Therefore, it was expected that complex **1** with a quaternary ammonium salt group, which does not take part in protonation/deprotonation equilibria, would not exhibit such behavior. Indeed, complex **1** exhibits minimal changes in the ratio of the bands at 588 and 527 nm in response to changes in pH of the solution from 5.5 to 9.5 (**SI Figure 5**).

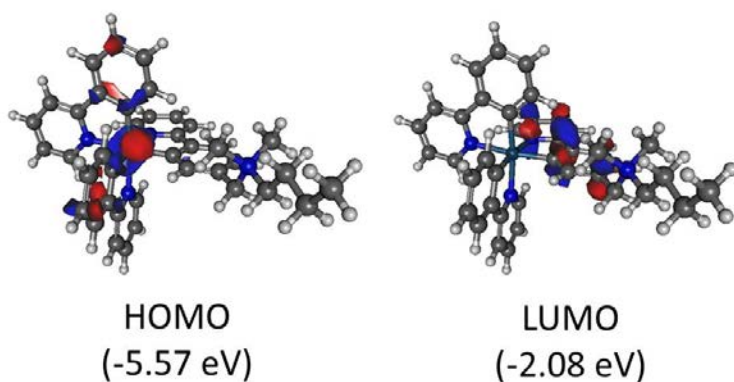
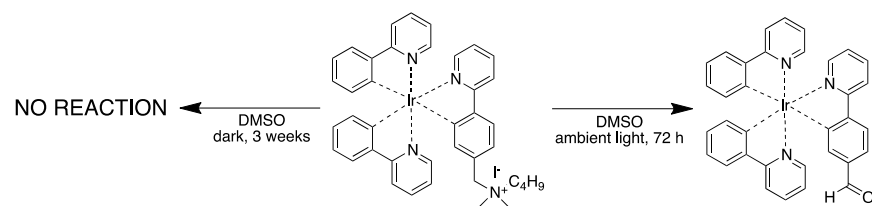


Figure 3. The HOMO and LUMO orbitals of complex **1** calculated in dichloromethane

Density Functional Theory (DFT) calculations for complex **1** were carried out using the polarizable continuum model as an approximation for solution in dichloromethane. The calculations were carried out at the B3LYP/LANL2DZ level of theory. The results shown in **Figure 3** indicate that the HOMO orbital is predominantly located on the iridium atom while the LUMO orbital localizes mainly on the substituted phenylpyridine ligand. This is in line with the expected MLCT nature of the transitions observed in the photophysical properties of such complexes. The energy difference between the two states (3.49 eV) is in line with the observed absorption spectrum. The geometry and orbital localization for the HOMO orbital of the T1 state can be seen in **SI Figure 6**. The electrons in this state are also located on the substituted phenylpyridine ligand indicating MLCT character of the emission. The calculated energy difference between this state and the singlet HOMO state (2.16 eV) is also in line with the observed emission.

Photoreactivity

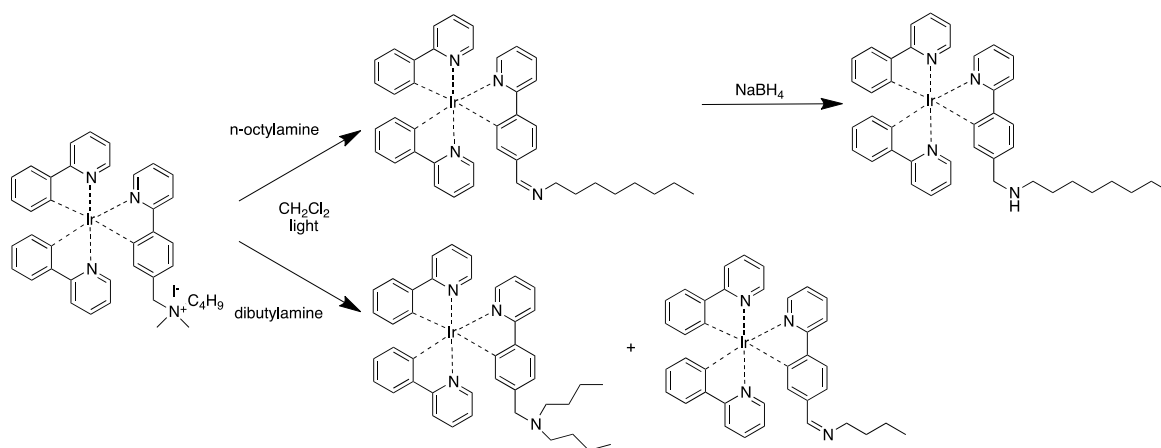
As mentioned above, the inability to purify complex **1** by column chromatography and its decomposition in an NMR sample indicated potential stability issues with this compound. ¹H-NMR analysis of the decomposed sample indicated that the product formed in this process is the precursor complex [Ir(ppy)₂fppy]. Subsequent experiments, where different solutions of complex **1** in DMSO were simultaneously kept in dark and irradiated by ambient light in the laboratory, provided evidence suggesting that the observed reactivity was indeed promoted by light. It was observed, using mass spectroscopy, that complex **1** kept in solution in dark remained intact for more than 3 weeks (**SI Figure 7, SI Table 1**). On the other hand, decomposition was observed in the solution kept in light within hours **Scheme 3 (SI Figure 8, SI Table 1)**. It is presumed that the reaction might proceed through an oxidative quench of the excited state of the complex by the quaternary ammonium moiety (**SI Scheme 1**).^[3, 26] This step would lead to the cleavage of the C-N bond and produce a benzylic radical on the benzylic position of the iridium complex and oxidize the iridium center to oxidation state +4. Similar reductive decomposition of quaternary ammonium salts has been observed in electrochemical studies.^[27, 28] Subsequent one electron transfer from the benzylic radical to the iridium center would lead to restoring of oxidation state +3 on the iridium center and formation of an electrophilic benzylic cation that could be involved in a reaction with various nucleophilic species, which could be water present in the DMSO solvent in this case. It should also be noted that the reactions were performed in the presence of oxygen, which is the likely reason for the observation of oxidation of the initial product from containing a hydroxy methyl group to the formyl group in [Ir(ppy)₂fppy] (**SI Figure 8**). The formation of this precursor complex was confirmed ¹H-NMR of the reaction mixture (**SI Figure 9**) with the appearance of the aldehyde peak at 9.62 ppm. In addition, the appearance of an emission peak at 605 nm (**SI Figure 10**), which corresponds to the emission of [Ir(ppy)₂fppy], provides further evidence.



Scheme 2. Photo transformation of complex **1**

To gain further understanding, the reaction was then carried out in dichloromethane, methanol, and acetonitrile to evaluate the effect of the solvents. In all cases, the solution kept in dark did not undergo decomposition of complex **1**, providing further support for the light induced nature of the transformation. Different products have been observed in these reactions. In the reaction carried out in dichloromethane, formation of $[\text{Ir}(\text{ppy})_2\text{fppy}]$ was observed (**SI Figure 11**, **SI Table 1**). The reaction in methanol lead to the formation of the corresponding methyl ether (**SI Figure 12**, **SI Table 1**). Finally, the reaction in acetonitrile lead to formation of several unidentified products as well as of the corresponding alcohol (**SI Figure 13**, **SI Table 1**).

The presumed involvement of electrophilic species in the photodegradation reactions described above suggested the possibility that such species could undergo reactions with other nucleophiles. Therefore, reactions with benzylamine, benzyl alcohol, and benzyl hydrosulfide were carried out as models for reactions with N, O, and S nucleophiles. These experiments have been carried out using a household lamp with an LED bulb to ensure more controlled irradiation. Reactivity was observed in all cases. However, only the reactions with benzylamine and benzyl alcohol resulted in formation of discernable products. The product formed when the reaction was carried out in the presence of benzylamine was the corresponding benzylidene imine (**SI Figure 14**, **SI Table 1**). This observation is in line with the presumed mechanism involving the formation of an electrophilic species, its capture by a nucleophile, and subsequent oxidation. The reaction with benzyl alcohol resulted in the formation of the corresponding ether (**SI Figure 15**, **SI Table 1**). The reaction was then performed with several other amines leading to similar observations. Interestingly, while the reaction with octylamine resulted in the formation of the corresponding imine as in the previous reactions (**SI Figure 16**, **SI Table 1**), reaction with dibutylamine resulted in the formation of both the tertiary amine and an imine where one of the butyl groups has been removed from the nitrogen atom (**Scheme 3**, **SI Figure 17**, **SI Table 1**).



Scheme 3. Photo transformation of complex **1** in the presence of primary and secondary amine

Further experiments with octylamine and dibutylamine were carried out to investigate the effect of reaction time. It was observed that the reaction mixtures contained the corresponding imine in the case of octylamine and the corresponding amine in the case of dibutylamine already after 15 minutes of irradiation (**SI Figure 18**, **SI Figure 19**, **SI Table 1**). It was only at this time point that the presence of the starting material could be detected. After 30 minutes of irradiation the reaction mixture containing dibutylamine exhibits the presence of the minor imine product formed after cleavage of the C-N bonds to one of the butyl groups (**SI Figure 20**). The reaction mixture containing octylamine displayed little change from the previous time point (**SI Figure 21**). Finally, when sodium borohydride was added to the reaction mixture formed after irradiation of complex **1** in the presence of octylamine the expected amine product was observed (**Scheme 3**, **SI Figure 22**). Overall these experiments suggest the possibility to use this reactivity for further structural modification of complex **1**, which will be investigated in the future.

Cellular Experiments

The main purpose for the synthesis and investigation of complex **1** was to test it as a potential cellular stain for live-cell fluorescence microscopy. The investigation of the behavior of complex **1** in cells was performed in NIH-3T3 cells. Initially, the cytotoxicity of complex **1** was investigated. The plot of cell viability of the NIH-3T3 as a function of concentration of complex **1** for 1h and 24h exposure can be seen in **Figure 4**. The IC_{50} values for 1h and 24 h exposure are more than $50 \mu\text{M}$ and $20 \mu\text{M}$, respectively. These results show that complex **1** is significantly less toxic than the precursor amine complex, which showed IC_{50} values below $10 \mu\text{M}$. Cell uptake

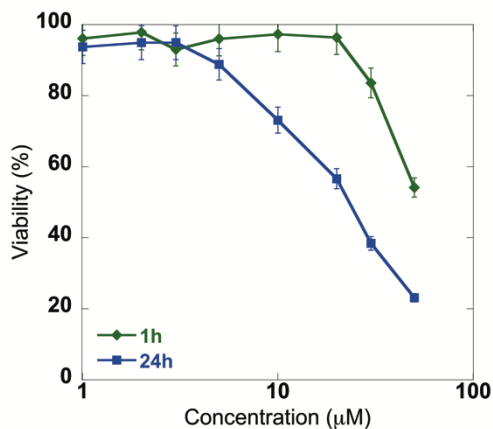


Figure 4. Plot of cellular viability of NIH-3T3 cells versus concentration of complex **1**

The potential of complex **1** to act as a cellular stain was then investigated using laser scanning confocal microscopy to evaluate its ability to enter cells and its subcellular localization properties. The imaging experiment was carried out after loading the cells with 5 μM solution of the complex for 1h. The ability of complex **1** to cross cellular membranes can be seen from **Figure 5a**. The cellular localization of complex **1** was compared to that of lysotracker red (**Figure 5b**). Good overlap ($P > 0.80$) of both channels was observed (**Figure 5c**) supporting lysosomal localization of complex **1**.

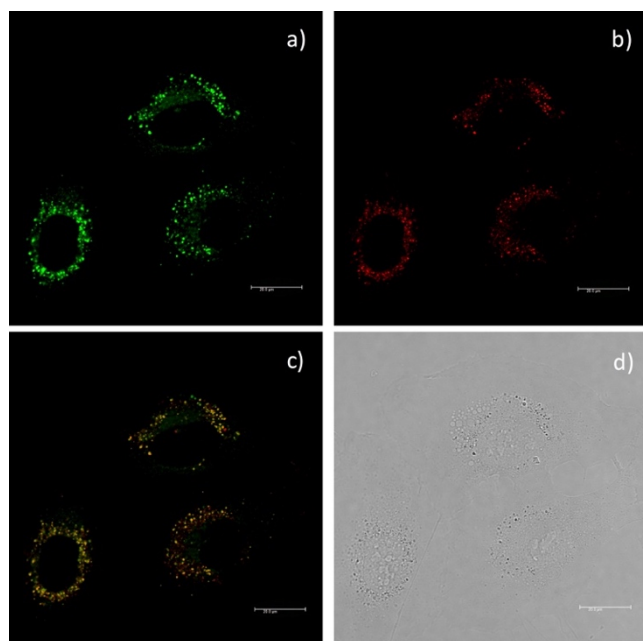


Figure 5. Fluorescence microscopy images of NIH-3T3 cells obtained with complex **1** (λ_{ex} 355 nm, λ_{em} 450-650 nm) (a), lysotracker red (λ_{ex} 543 nm HeNe laser, λ_{em} 600-650 nm) (b). Panel c shows the RGB overlay of panels a and b; $P = 0.80$, while panel d is the brightfield image. (Scale bar: 20 μm)

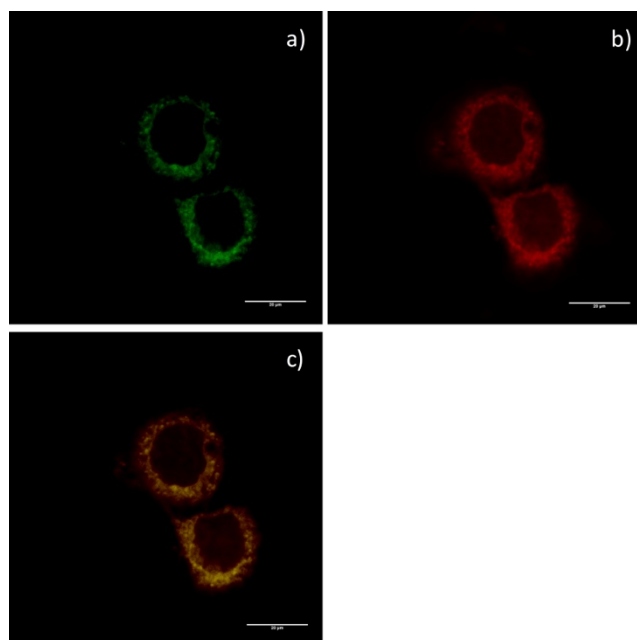


Figure 6. Two photon microscopy images of NIH-3T3 cells incubated with complex **1** and acquired at 720 nm excitation, with emission collected using a 510 nm long-pass filter (a), lysotracker red (λ_{ex} 960 nm, λ_{em} 580 nm long-pass filter) (b). Panel c shows the RGB overlay of panels a and b; $P = 0.68$. (Scale bar: 20 μm)

Emission spectra were recorded for cell lysate and are shown in **Appendix Figure 23**. These are similar to those observed in solution indicating the integrity of the iridium coordination sphere after internalization in the cells. In addition, the brightness of cell images for cells loaded with complex **1** (5 μM for 24h), was 680% higher than that of blank cells, which supports the presence of emissive cyclometalated iridium complex in the cells. Uptake of complex **1** was evaluated using ICP-MS analysis of cell lysates for the presence of iridium after their exposure to 5 μM solution of complex **1** for 24 h. The observed intracellular iridium concentration was 3.4 μM , which is significantly higher than that for blank sample, further supporting the ability of complex **1** to translocate across the cell membrane. It should be noted that the amine precursor complexes show more efficient cell uptake than complex **1**, which is approximately two fold higher, it is unlikely that this is the only reason for the decreased cytotoxicity of complex **1**.

Finally, the possibility to perform imaging with complex **1** using two photon excitation was evaluated. The imaging was performed using excitation at 720 nm and the image is shown in **Figure 6**. The lower overlap of the emission of the complex and the lysotracker red dye and the overall less-defined granular appearance of its lysosomal localisation in the two-photon image ($P=0.68$), in comparison to the single photon image in **Figure 5**, is caused by lower spatial resolution of the two-photon imaging system.

Conclusions

In conclusion, a novel tris-cyclometalated iridium complex (**1**) containing a quarternary ammonium group has been synthesized and investigated. The complex shows good photophysical properties enabling its use as a cellular stain in fluorescence microscopy.

Cellular imaging experiments have demonstrated that the complex is less toxic than its secondary amine precursor, which was previously reported by our group, but shows lysosomal localization as this previously reported complex. The ability possibility to perform two-photon imaging with complex **1** has been demonstrated as well. However, complex **1** exhibits rapid photoreactivity, which, even though it does not preclude performing the imaging experiments, limits its practical utility for this purpose. On the other hand, it was demonstrated that this photoreactivity can be used for the formation of new products. The utilization of the this reactivity, including for the purpose of N-tagging, will be investigated in the future.

Acknowledgements

This research was supported a grant from the Thailand Research Fund No. RSA6080041. The authors also acknowledge the National e-Science Infrastructure Consortium. S.M. also acknowledges scholarship support from the Science Achievement Scholarship of Thailand (SAST). RP acknowledges support from the Royal Society University Research Fellowship.

References

- [1] Y. You, *Current opinion in chemical biology*, 17 (2013) 699-707.
- [2] Y. You, W. Nam, *Chemical Society reviews*, 41 (2012) 7061-7084.
- [3] B. König, *European Journal of Organic Chemistry*, 2017 (2017) 1979-1981.
- [4] M.H. Shaw, J. Twilton, D.W.C. MacMillan, *The Journal of organic chemistry*, 81 (2016) 6898-6926.
- [5] Y.-X. Hu, X. Xia, W.-Z. He, Z.-J. Tang, Y.-L. Lv, X. Li, D.-Y. Zhang, *Organic Electronics*, 66 (2019) 126-135.
- [6] T.-Y. Li, J. Wu, Z.-G. Wu, Y.-X. Zheng, J.-L. Zuo, Y. Pan, *Coordin Chem Rev*, 374 (2018) 55-92.
- [7] S. Ladouceur, E. Zysman-Colman, *Eur J Inorg Chem*, 2013 (2013) 2985-3007.
- [8] K.P. Zanoni, R.L. Coppo, R.C. Amaral, N.Y. Murakami Iha, *Dalton Trans*, 44 (2015) 14559-14573.
- [9] F.L. Thorp-Greenwood, R.G. Balasingham, M.P. Coogan, *J Organomet Chem*, 714 (2012).
- [10] D.N. Chirdon, W.J. Transue, H.N. Kagalwala, A. Kaur, A.B. Maurer, T. Pintauer, S. Bernhard, *Inorganic chemistry*, 53 (2014) 1487-1499.
- [11] Y. You, J. Seo, S.H. Kim, K.S. Kim, T.K. Ahn, D. Kim, S.Y. Park, *Inorganic chemistry*, 47 (2008) 1476-1487.
- [12] C.-J. Li, S.-Y. Yin, H.-P. Wang, Z.-W. Wei, M. Pan, *Journal of Photochemistry and Photobiology A: Chemistry*, 379 (2019) 99-104.
- [13] C. Caporale, M. Massi, *Coordin Chem Rev*, 363 (2018) 71-91.
- [14] M.P. Coogan, V. Fernandez-Moreira, *Chem Commun (Camb)*, 50 (2014) 384-399.
- [15] V. Fernandez-Moreira, F.L. Thorp-Greenwood, M.P. Coogan, *Chem Commun (Camb)*, 46 (2010) 186-202.
- [16] D.L. Ma, S.Y. Wong, T.S. Kang, H.P. Ng, Q.B. Han, C.H. Leung, *Methods*, (2019).
- [17] M. Zang, H. Su, L. Lu, F. Li, *Talanta*, 202 (2019) 259-266.
- [18] S. Aoki, Y. Matsuo, S. Ogura, H. Ohwada, Y. Hisamatsu, S. Moromizato, M. Shiro, M. Kitamura, *Inorganic chemistry*, 50 (2011) 806-818.
- [19] Y. Hisamatsu, A. Shibuya, N. Suzuki, T. Suzuki, R. Abe, S. Aoki, *Bioconjug Chem*, 26 (2015) 857-879.

- [20] A. Sansee, S. Meksawangwong, K. Chainok, K.J. Franz, M. Gal, L.O. Palsson, W. Puniyan, R. Traiphol, R. Pal, F. Kielar, *Dalton Trans*, 45 (2016) 17420-17430.
- [21] G.W.T. M. J. Frisch, H. B. Schlegel, G. E. Scuseria, M. A. Robb, J. R. Cheeseman, G. Scalmani, V. Barone, B. Mennucci, G. A. Petersson, H. Nakatsuji, M. Caricato, X. Li, H. P. Hratchian, A. F. Izmaylov, J. Bloino, G. Zheng, J. L. Sonnenberg, M. Hada, M. Ehara, K. Toyota, R. Fukuda, J. Hasegawa, M. Ishida, T. Nakajima, Y. Honda, O. Kitao, H. Nakai, T. Vreven, J. A. Montgomery, Jr., J. E. Peralta, F. Ogliaro, M. Bearpark, J. J. Heyd, E. Brothers, K. N. Kudin, V. N. Staroverov, T. Keith, R. Kobayashi, J. Normand, K. Raghavachari, A. Rendell, J. C. Burant, S. S. Iyengar, J. Tomasi, M. Cossi, N. Rega, J. M. Millam, M. Klene, J. E. Knox, J. B. Cross, V. Bakken, C. Adamo, J. Jaramillo, R. Gomperts, R. E. Stratmann, O. Yazyev, A. J. Austin, R. Cammi, C. Pomelli, J. W. Ochterski, R. L. Martin, K. Morokuma, V. G. Zakrzewski, G. A. Voth, P. Salvador, J. J. Dannenberg, S. Dapprich, A. D. Daniels, O. Farkas, J. B. Foresman, J. V. Ortiz, J. Cioslowski, and D. J. Fox, in: *Gaussian 09*, Gaussian, Inc., Wallingford, CT, USA, 2009.
- [22] A.A. R., *Journal of Computational Chemistry*, 32 (2011) 174-182.
- [23] R. Pal, *Faraday Discuss*, 177 (2015) 507-515.
- [24] M. Nonoyama, *Bulletin of the Chemical Society of Japan*, 47 (1974) 767-768.
- [25] A. Beeby, S. Bettington, I.D.W. Samuel, Z. Wang, *J Mater Chem*, 13 (2003) 80-83.
- [26] S.Z. Zard, *Radical Reactions in Organic Chemistry*, Oxford University Press, New York, 2003.
- [27] J.S. Mayell, A.J. Bard, *Journal of the American Chemical Society*, 85 (1963) 421-425.
- [28] M.P.S. Mousavi, S. Kashefolgheta, A. Stein, P. Bühlmann, *Journal of The Electrochemical Society*, 163 (2016) H74-H80.